Engineering and Technology Journal
Journal homepage: https://etj.uotechnology.edu.iq

Experimental and numerical investigation of Al_2O_3-SiO_2 Nanopowder for stainless steel 304 L

Qasim A. Sachit[a]*, Maan A. Tawfiq[a]*, Muhssn H. Shamky[b], Waseem M. Abbas[b]

[a]Production Engineering and Metallurgy Dept., University of Technology-Iraq, Alsinaa street, 10066 Baghdad, Iraq.
[b]Midland Refineries Company, Ministry of Oil – Iraq.
*Corresponding author Email: Maan.A.Tawfiq@uotechnology.edu.iq

HIGHLIGHTS

- The effect of Al_2O_3-SiO_2 nanopowder on machining stainless steel 304L was experimentally investigated.
- MRR, EWR, and Ra were measured to evaluate the machining performance using nanopowder-mixed EDM.
- RSM was applied to model the relationship between inputs and outputs in the NPMEDM process.
- Surface response optimization increased MRR by 13% and reduced EWR and Ra by 33.3% and 4.5%, respectively.

Keywords:

Electrical Discharge Machining
Stainless Steel 304L
NPMEDM
Al_2O_3
SiO_2

ABSTRACT

Electro-Discharge Machining (EDM) is a unique manufacturing method. Recently developed thermo-electric methods include Nano Powder-Mixed Electric Discharge Machining (NPMEDM), which suspends metallic Nanopowder in a dielectric. This study examines how Al_2O_3 -SiO_2 Nanopowder concentration and mixing ratio affect EDM dielectric fluid surface integrity (outputs) on stainless steel 304L. Material Removal Rate (MRR), Electrode Wear Rate (EWR), and surface roughness (Ra) are used to evaluate machining efficiency. Nanofluid has much better heat conductivity than dielectrics, enhancing material removal. Material Removal Rate rises with discharge current. At Run No. 26, increasing Al_2O_3 particle proportion with 35 A discharge current, 2 g/l particle concentration, 200 µs pulse on time, and 50 µs pulse off time increases material removal rate by 13%. Increasing discharge currents lowers Ra. Lowering discharge current to 20 A, particle concentration to 3 g/l, pulse on time to 150 µs, and pulse off time to 75 µs lowered aluminium oxide particle composition to 50%, increasing Ra by 4.5% at Run No. 37. Increased discharge currents lower EWR. By increasing discharge current to 25 A, particle concentration to 4 g/l, pulse on time to 200 µs, and pulse off time to 100 µs, aluminium oxide particle composition was reduced to 40%, leading to a 33.3% rise in EWR at Run No. 50 using Design Expert 11 software. Current 37.8%, pulse on 12.6%, nanopowder concentration 3%, and pulse off 25.85% are needed for MRR. The mixing ratio parameter does not affect MRR. EWR needs 25.5% current and 25.6% nanopowder. Ra depends on nanopowder concentration, peak current at 4.5%, pulse-off duration at 20.24%, current-pulse duration at 7.6%, and current-pulse off duration at 37.9%.

1. Introduction

Most people today rely on EDM for complex jobs requiring tough materials such as stainless steel 304L machining. The invention of NPMEDM has resulted from adding nanoparticles of Al_2O_3 or SiO_2 to the dielectric in the process, which improves heat distribution, the flow of sparks, and overall EDM machining results [1]. Even though adding nanopowder to MMW is known to improve MRR and Ra, experts still do not fully understand how input values such as nanopowder dosage, mix ratio, current, and pulse durations impact EWR and the quality of the surface [2]. The condition of surfaces and the wear of tools contrast in different ways as the Al_2O_3–SiO_2 nanopowder compositions change, and errors still occur between experiment runs. For instance, the material removal rate may improve when you use extra discharge current and a higher amount of nanopowder. Still, the etching time of the substrate sometimes increases or the finish on the surface degrades, depending on various conditions. There seems to be a relationship here that has not been used for industrial purposes as much, and may depend on different situations. In addition, the effect of nanopowder mixing ratio on EDM results is less understood, and there is insufficient evidence about its importance [3].

Hence, we need to look into how the amount and structure of Al_2O_3–SiO_2 nanopowder, EDM process settings, and other variables influence stainless steel 304L by using Design Expert software. Doing such analysis is crucial for improving the trustworthiness, productivity, and continuous improvements in mean residence time, equipment waste ratio, and reliability.

http://doi.org/10.30684/etj.2025.149443.1813
Received 05 May 2025; Received in revised form 05 June 2025; Accepted 20 June 2025; Available online 21 September 2025
2412-0758/University of Technology-Iraq, Baghdad, Iraq

Electricity significantly enhanced the MRR while diminishing the EWR and SR. Effectively leveraging the capabilities of diverse unconventional machining processes requires the meticulous selection of the most suitable strategy for a specific application [4]. EDM is one of the most widely utilized unique machining processes. This process has effectively replaced previous techniques for cutting hard materials. Historically, the EDM method was restricted to the machining of electrically conductive materials; however, advancements in technology today allow for the machining of ceramics and composites. It produces intricate shapes, irregular proportions, elaborate decorations, and minuscule apertures [5]. The evaluation of EDM performance is conducted using MRR (material removal rate), EWR (electrode wear rate), SR (surface roughness), and other machining responses [6]. EDM is utilized across multiple sectors, such as gear manufacture, mold and die fabrication, aerospace, automotive, biotechnology, sports, electronics, medical, jewelry, and toys, with enhancements achieved through the incorporation of SiO2-graphite nanopowder to augment performance [7-11]. The impact of mixing powder into the dielectric fluid on the efficiency of the EDM process was examined by several researchers [12-24]. The process is known as powder mix electrical discharge machining, or PMEDM. Tungsten [20, 21], chromium [22], titanium [23,24], silicon [16,17], silicon carbide [18,19], graphite [14,15], aluminum [12,13], and other powders have been tried. According to these experiments, the EDM dielectric's machining efficiency, surface finish, and material removal rate are all enhanced by adding powder. The size of the particles may range from micro to nano. Some EDM experiments have employed CNT and nanopowder mixed dielectric. Use nanopowders from CNTs and other materials. Application possibilities for carbon nanotubes are vast. Strong, stiff, durable, and electrically and thermally conductive. Multilayer graphite tubes make up MWCNTs. This research aimed to determine how CNT and nanopowder mixed dielectric fluids affect EDM performance. Electrical discharge machined SKD-11 surface properties were examined about dielectric fluid particle size. Powder additives: aluminum, chromium, copper, and silicon carbide. Smaller particles (70-80 nm) produce better surfaces. Smaller particles produced a thicker recast layer [25].

The study examined the influence of powder additives suspended in dielectric fluid on crater features during micro-electrical discharge machining of stainless steel. Daphne Cut HL-25 dielectric fluid and SiC nanopowder (45-55 nm) were utilized. Transferring charges between the tool and the workpiece was reduced, leading to a uniform depth and diminished crater size. A smaller crater containing a greater volume of re-solidified material was identified within the crater chamber [26], and the effect of nanopowder suspended in dielectric fluid on the surface roughness of AISI 420 stainless mold steel during micro-EDM was investigated. Idemitsu Daphne Cut HL25-S dielectric fluid, silicon carbide, and aluminum oxide particulates were utilized. The tool electrode consisted of tungsten. Surface roughness was reduced utilizing SiC and Al_2O_3 microparticles [27]. The AISI D2 tool steel's surface properties were analyzed using the EDM technique. Machining was performed using a copper electrode and single-walled carbon nanotubes (SWCNT) suspended in kerosene dielectric. It was disclosed that workpieces machined with SWCNT-infused dielectric exhibited superior surface quality and a reduced incidence of microcracks. Configuring the machine parameters to low pulse energy yielded an exceptional machined nano finish [28]. The study examined the enhancement of surface properties in cemented tungsten carbide micro-EDMs by incorporating graphite nanopowder into the dielectric. A tungsten tool and an oil dielectric known as "Total FINA ELF EDM3" were utilized. Surface quality and material removal rate were enhanced, while the tool wear rate diminished. The increased spark gap improved surface topography and crater distribution [29]. The investigation focused on nano graphite powder suspended in kerosene dielectric during the micro-electrical discharge machining of silver-tungsten workpieces. The tool's material was tungsten, with a particle size of 55 nm. Improvements in surface quality and machining duration were identified. The nano graphite powder dispersion particle size resulted in a significant spark gap, reducing electric discharge power density and diminishing explosive force [30]. The efficacy of EDM operations in milling Inconel 718 was examined utilizing kerosene dielectric infused with titanium carbide nanopowder. A brass implement was utilized for machining. The incorporation of nanopowder enhanced material removal rate (MRR) while reducing tool wear rate (TWR) [31] utilizing multi-walled carbon nanotubes (MWCNTs) in the dielectric fluid for machining Al-10% SiCp metal matrix composites (MMCs) during EDM. Copper was utilized as a tooling material throughout the machining process. Incorporating MWCNTs into the dielectric fluid significantly enhanced the material removal rate (MRR) and surface quality [32]. Adding carbon nanotubes to the oil flux ELF2 dielectric during Ti-6Al-4V EDM was studied. This experiment used copper tools. Using carbon nanotubes with dielectric materials reduced surface microcracks. CNTs reduced MRR, TWR, and SR [33]. EDM using a dielectric and Al_2O_3 nanopowder was tested for grinding Inconel 825. MRR and surface roughness increased significantly when nanopowder was added to deionised water dielectric fluid. A copper machining tool. In industry, cheap Al_2O_3 powder works well [34]. Graphite nanopowder-infused EDM fluid dielectric affects Inconel 718 micro-wire electrical discharge machining [35].

Nanofluids consist of dielectric particles with dimensions ranging from 1 to 100 nanometers. Nanoparticles possess a singular characteristic: a high surface area to volume ratio, dimensionally dependent physical characteristics, and reduced kinetic energy. The most fascinating feature of nanofluids is that a minimal addition of nanoparticles leads to a tenfold enhancement in thermal conductivity above theoretical expectations. Incorporating 0.3 vol.% copper nanoparticles into ethylene glycol enhanced its thermal conductivity by 40% [36]. Heat transfer fluids (HTFs) are utilized in diverse industrial and municipal applications, including air conditioning, transportation, energy provision, and electronic cooling. Water, oils, glycols, and fluorocarbons exemplify earlier heat transfer fluids with low thermal conductivities. Efforts in research and development were undertaken to enhance the thermal conductivity of liquids. Solid metallic substances like silver, copper, and iron, along with nonmetallic materials such as alumina, CuO, SiC, and carbon nanotubes, exhibit far greater thermal conductivities than earlier heat transfer fluids, which incorporated solid particles of micron or millimeter dimensions with base fluids or slurries. Large solid particles, conversely, cause surface abrasion, microchannel blockage, pipeline corrosion, and heightened pressure loss, thus restricting potential uses [37]. Surface polishing utilizing nanopowder decreased the average surface roughness. The machined surface exhibited no minute fractures. Inconel superalloys are nickel-based alloys employed in high-pressure and high-temperature applications, including gas turbines, electric power generation systems, nuclear reactors, and high-temperature chemical vessels [38]. Numerous studies investigate the impact of nanoparticle incorporation on SR. Al_2O_3 and silicon carbide nanoparticles were found to reduce the surface roughness of stainless steel micro-electrical discharge machining[39,40].

This study focuses on the highly challenging material stainless steel 304L. Machining this material using conventional methods may damage the tool and induce internal stresses in the workpiece. The research also investigates how Electrical Discharge Machining (EDM) addresses these issues. By optimizing the input process parameters, the study also aims to enhance the material removal rate (MRR), reduce surface roughness, and minimize the electrode wear rate (EWR).

2. Materials and methods

2.1 Workpiece characterization and machining

Stainless steel 304L was used in this study as a workpiece. Nanoparticles were made from aluminum oxide (Al_2O_3) and silicon dioxide (SiO_2). They use a 1 - 5 g/l concentration and a mix fraction of 30 - 70% Al_2O_3 with SiO_2 balanced to integrate with kerosene dielectric. Figure 1a shows the workpiece dimensions (25.4 mm diameter x 5 mm thickness). Kerosene is utilized as a dielectric fluid. Figure 1b shows how the tests are carried out using a cylindrical copper electrode with a diameter of 16 mm and a length of 40 mm.

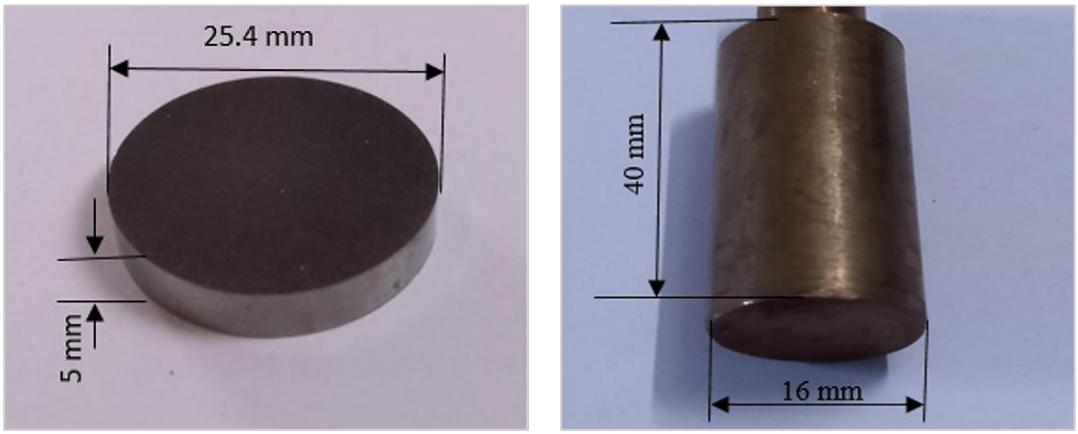

(a) **(b)**

Figure 1: a) Workpiece before machining (25.4 mm diameter x 5mm Thickness) b) Copper electrode (16 mm diameter x 40 mm length)

EDM is a precise manufacturing technology for shaping hard, electrically conducting materials. Traditional machining employs mechanical cutting, but EDM uses electrical sparks to dissolve material. Tool and workpiece electrodes are submerged in dielectric fluid. A voltage causes regulated electrical discharges between the electrodes, generating intense heat that melts and vaporizes small parts of the workpiece-cooling and flushing trash with dielectric fluid. Sinker, wire, and hole drilling EDM machines exist. Mould and die makers utilize sinker EDM to build complicated cavities using a shaped electrode. Wire EDM, which uses a thin wire electrode, cuts accurate forms well. Hole drilling EDM makes deep, tiny holes in turbine blades and other hard materials. EDM can manufacture extremely hard materials without mechanical stress and generate complicated shapes. Its slower removal rates and electrically conductive material limits are drawbacks. Despite these drawbacks, EDM is popular in businesses that need precise machining of difficult parts. The machining properties of stainless steel 304L are investigated utilizing the electric discharge machining (EDM) process. The current study's tests were carried out on a numerically controlled electric discharge machine with the model number [CM 323+50N (CHAMBER EDM)] (Taiwanese origin). Fifty trials were conducted with identical input process settings and conditions for NPMEDM. The results were discussed using measured material removal rate, electrode wear rate, and surface roughness values. Figure 2 depicts the machined workpiece.

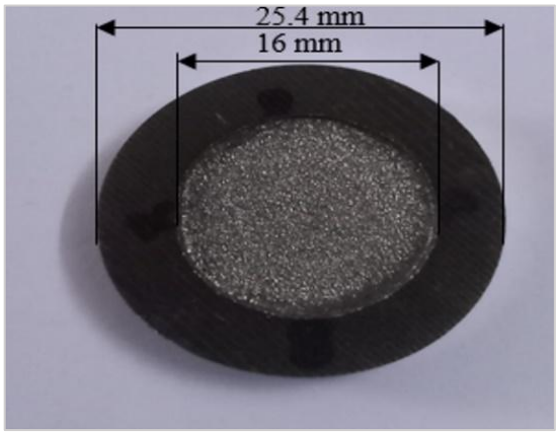

Figure 2: Workpiece after machining

Table 1 demonstrates complete measurements and thermo-physical properties of the selected electrode. Table 2 shows the chemical composition of the workpiece (stainless steel 304L) and the electrode characteristics. This experiment was done by mixing 20-nm aluminum oxide particles and 50-nm silicon dioxide with a kerosene dielectric. Table 3 shows some of the critical and effective Nanopowder specifications used in the NPMEDM process.

Table 1: Specifications and Thermophysical properties of the copper electrode

Diameter of tool (mm)	**16**
Tool length (mm)	40
Specific heat capacity (J/kg-ºC)	385
Thermal conductivity (W/m-ºC)	385
Thermal diffusivity (m^2/s)	1.11×10^{-4}
Density (Kg/m^3)	8960
Melting point (ºC)	1085
Thermal expansion coefficient at 20 ºC (/ºC)	16.5×10^{-6}

Table 2: Chemical composition of stainless steel 304 L

Chemical element	**Cr**	**Ni**	**Mn**	**Cu**	**Si**	**P**	**Ni**	**C**	**S**	**Fe**
% Composition	18.37	8.19	1.8	0.58	0.54	0.039	0.037	0.021	0.019	Balance

Table 3: The effective physical properties of nanoparticles in NPMEDM

Nanoparticles	**Density(g/cm^3)**	**Thermal Conductivity (W/cmK)**	**Electrical Resistivity (μΩ.cm)**	**Particle size (nm)**
Al_2O_3	1.8	5	10^4	50
SiO_2	2.4	1.3	10^8-10^{12}	50

Machining experiments using the response surface methodology (RSM) are conducted using the Design Expert 11. The study's input parameters included the electric discharge current, particle concentration, pulse on/off period, and nanoparticle mixing percentage. There were five levels of testing for each parameter. Table 4 contains a list of parameters and their respective ranges. Response characteristics include surface roughness (Ra), electrode wear rate (EWR), and material removal rate (MRR). The weight loss method was used to compute the MRR and EWR. The SR was measured using the Pocket Surf (Mahr FEDERAL) device tester (American origin), which averages three measurements from the cutting surface in different directions. Additionally, alumi num oxide Nanopowder is used in studies as a basis for determining particle composition percentage. The low-voltage mode EDM machine was used for all experiments.

Table 4: Parameters and their levels

		Levels				
No.	**Parameters**	**1**	**2**	**3**	**4**	**5**
1	Pulse off time (μs)	25	50	75	100	125
2	Pulse on time (μs)	50	100	150	200	250
3	Peak current (A)	20	25	30	35	40
4	Mix of powder (% Al_2O_3)	30	40	50	60	70
5	Concentration (g/l)	1	2	3	4	5

3. Equipment of measurement

3.1 Weight balance

The weight of the workpiece and electrode was determined using a high-precision balance, and its specifications are demonstrated in Table 5. The apparatus has a capacity of 300 grams and an accuracy of 0.001 grams and belongs to the Brand Model JM-B (German origin).

Table 5: Specification of the Weight Balance

Specification	**Value**
Max. Capacity	220 g
Readability	0.1 mg
Repeatability	0.1 mg
Weighing pan area	80 mm diameter

Equations 1 and 2 compute the material removal rate (g/min) and electrode wear rate (g/min) due to machining time, respectively.

$$MRR = \frac{InitialWeightofwork - FinalWeightofwork}{MachiningTime} \quad (1)$$

$$EWR = \frac{InitialWeightofElectrode - FinalWeightofElectrode}{MachiningTime} \quad (2)$$

3.2 Measurements of (Ra) and pocket surf

Surface roughness, measured by the center line average (R_a), is the average deviation of the roughness profile from the center line. Ra is expressed in Equation 3.

$$R_a = \frac{1}{l}\int y(x)dx \quad (3)$$

where, *l*: the sample length, *y:* the height of peaks and valleys of the roughness profile, *x:* the profile direction.

Surface roughness (Ra) was measured using a portable stylus-type profilometer. Table 6 contains the specifications of the Pocket Surf (Mahr FEDERAL) device (American origin).

Table 6: Specification of the roughness apparatus measurement

Specification	Value
Dimension	140 mm × 76 mm × 25 mm
Weight	435 g
Measuring Ranges	Ra 0.03 µm to 6.35 µm Ry 0.2 µm to 25.3 µm R_{max} 0.2 µm to 25.3 µm Rz 0.2 µm to 25.3 µm
Display Resolution	0.01 µm
Measurement accuracy	Meets ASME-B461, ISO, DIN standards, and MIL specifications.
Digital Readout	LCD with "Battery low" signal; "H" and "L" (measured value out-of-range).

3.3 Statistical analysis for NPMEDM process

The goodness of the second-order model and the evaluation of the dominant parameters of all output characteristics of the machining process were implemented according to (ANOVA) technique. ANOVA is used to test the resulting hypotheses at a confidence level of 95%. The Fisher statistical test (F-test) was adopted to determine the significance of the parameters. The maximum levels of the F-test indicate the more influential parameter, and the p-value for the F-statistic represents the probability of the measured data. If the p-value ≤ 0.05, the parameter has a statistically significant influence. The percentage of contribution of individual parameters can be determined from the ANOVA table by the following expression, Equation 4 [41]:

$$\text{Percentage contribution (C \%)} = \frac{Sum\ of\ Square\ of\ Variation}{Total\ Sum\ of\ Square\ of\ Variation} \times 100 \quad (4)$$

4. Results and discussion

4.1 RSM and regression model for MRR, EWR, and Ra

Response Surface Methodology (RSM) is a statistical technique to tackle complex multiple-response industrial problems. Response results are examined using the response surface methodology. The experimental protocols were created using Central Composite Design (CCD) concepts. Fifty full factorial experiments were carried out using the RSM design matrix developed. Peak current (I_p), pulse-on time (P_{on}), pulse-off time (P_{off}), powder concentration, and mixing ratio of powder are the five input process factors that are investigated in this study. Each of these parameters has been investigated at five different levels for testing. Measures including Material Removal Rate (MRR), Electrode Wear Rate (EWR), and Surface Roughness (SR) have been carried out using the response surface methodology. "Design Experts 11" is a highly renowned statistical software used to assess the responses in this discipline [42]. The relationship between the input variables and response characteristics of the machining process was determined and analyzed based on Regression analysis. A Non-linear equation represented the relation that connects the input parameters with the responses in the regression analysis. Depending on the experimental output values, RSM developed mathematical models, and the general 2nd-order model was developed and adopted in the present work. Equations (5), (6), and (7), shown below illustrate the mathematical models for the output required performance measures:

$$\begin{aligned}\text{Ra} = {} & 5.45534 + 0.1626\,\text{x A} + 0.00925\,\text{x B} + 0.34645\,\text{x C} + 0.12425\,\text{x D} + -0.06555\,\text{x E} + \\ & -0.236937\,\text{x AB} + 0.53\,\text{x AC} + -0.012125\,\text{x AD} + -0.0090625\,\text{x AE} + -0.139375\,\text{x BC} + \\ & -0.0035\,\text{x BD} + 0.0073125\,\text{x BE} + 0.0069375\,\text{x CD} + -0.009125\,\text{x CE} + 0.009125\,\text{x DE}\end{aligned} \quad (5)$$

$$\begin{aligned}\text{Sqrt(MRR)} = {} & 0.368258 + 0.041593\,\text{x A} + 0.0240059\,\text{x B} + -0.0343912\,\text{x C} + -0.00193682\,\text{x D} + \\ & 0.011716\,\text{x E}\end{aligned} \quad (6)$$

$$\text{WR} = 0.004826 + 0.00127\,\text{x A} + -2\text{e}-05\,\text{x B} + -0.00073\,\text{x C} + 0.000165\,\text{x D} + 0.001555\,\text{x E} \quad (7)$$

where, A: Current, B: Pulse on, C: Pulse off, D: Nanopowder Concentration, E: Nanopowder Mixing Ratio Al_2O_3 %-balanced SiO_2.

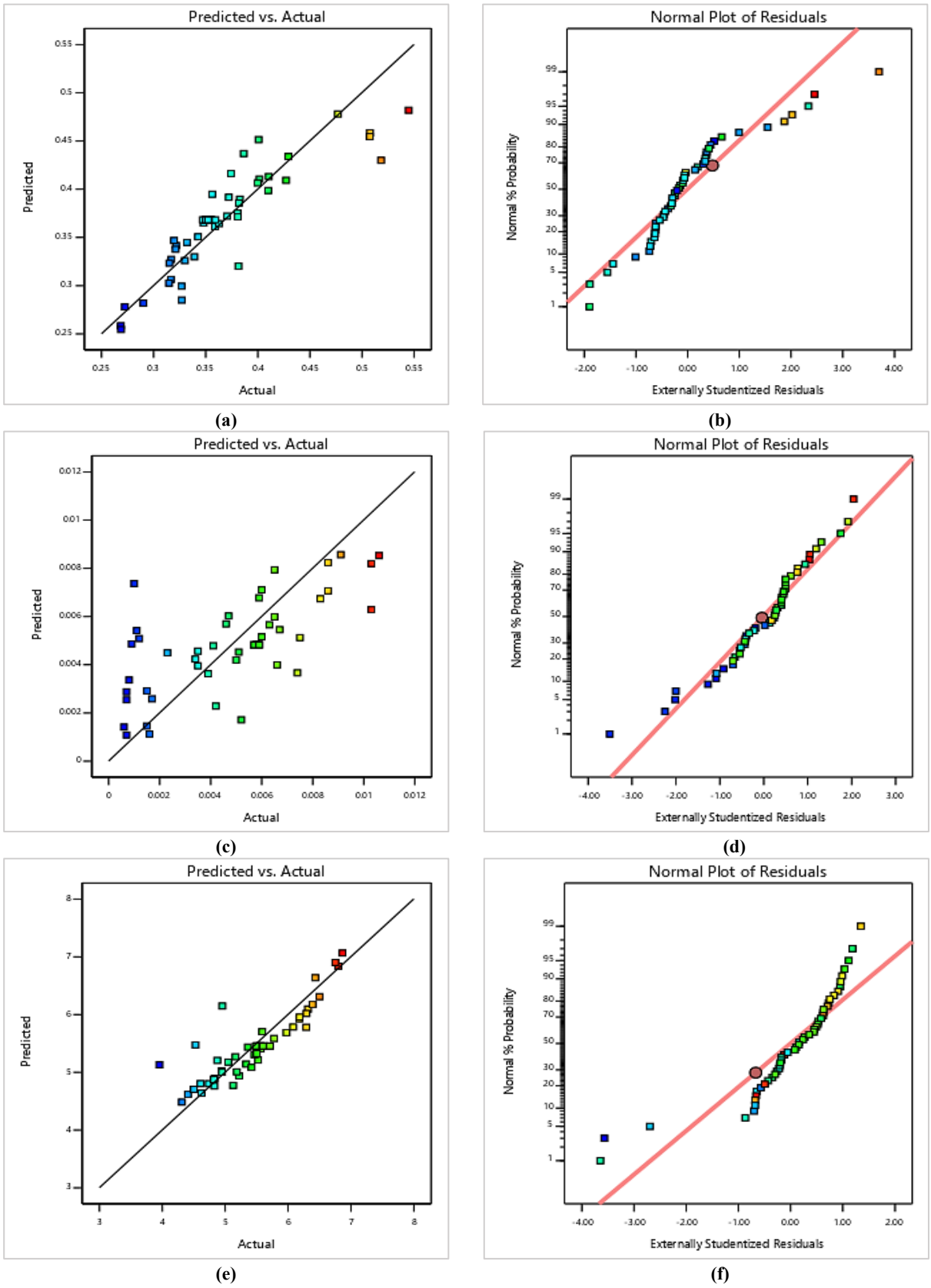

Figure 3: a) Predicted vs. Actual (Experiment) MRR b) Normal vs. Externally studentized residuals MRR c) Predicted vs. Actual (Experiment) EWR d) Normal vs. Externally studentized residuals EWR e) Predicted vs. Actual (Experiment) Ra f) Normal vs. Externally studentized residuals Ra

Equations determined the predicted MRR, EWR, and Ra values 4, 5, and 6. Based on the outputs, the precision of predicting the developed model appeared acceptable. Tables 7, 8, and 9 show the results of fifty runs' material removal rate, electrode wear rate, and surface roughness. Figures 3(a), 3(c), and 3(e) present the actual versus predicted values. The average probability plots for each mathematical model were performed as shown in the previous figures. Figures 3(b), 3(d), and 3(f) depict the average probability of the machining characteristics, which are utilized to check the normality assumption and the normal distribution of errors. Table 7 notes that the highest MRR is at Run No. 26 by 0.5449 g/min when the current (35 A), pulse on time (200 µs), pulse off time (50 µs), powder concentration (2 g/L), and mixing ratio (60% Al_2O_3 - 40% SiO_2). Through Table 8, we notice that the lowest EWR is at Run No. 50 by 0.0006 g/min when the current (25 A), pulse on time (200 µs), pulse off time (100 µs), powder concentration (4 g/L), and mixing ratio (40% Al_2O_3 - 60% SiO_2). Finally, from Table 9, we note that the lowest Ra is at Run No. 37 by (3.954 µm) when the current (20 A), pulse on time (150 µs), pulse off time (75 µs), powder concentration (3 g/L), and mixing ratio (50% Al_2O_3 - 50% SiO_2). The ratio of the standard deviation to the mean is known as the Coefficient of Variation, or CV. With an increasing coefficient of variation, the degree of dispersion around the mean increases. Generally, a percentage is used to express it. It enables comparison between distributions of values whose measurement scales are incomparable when no units are involved. The CV connects the estimate's value to the estimate's standard deviation when estimated values are given. The estimate is more accurate, and the coefficient of variation value is lower. CV (0.01–0.10): the result is excellent, (0.11-0.20): acceptable, (0.21-0.30): Poor result. The predicted MRR, EWR, and Ra values were determined by Equations (5), (6), and (7). Based on the outputs, the precision of predicting the developed model appeared acceptable.

4.2 Prediction Accuracy of MRR, EWR, and Ra

Table 7 presents the prediction accuracy of the square root of Material Removal Rate (MRR) for the NPMEDM process, based on 50 experimental runs. Various parameters were adjusted, including peak current (Ip), pulse-on time (Ton), pulse-off time (Toff), powder concentration, and the mixture ratio of Al_2O_3 to balanced SiO_2. The results show that the model's predicted MRR values are generally very close to the experimental values, with most error ratios between experimental and predicted results hovering around 1, indicating high prediction accuracy. Although most runs exhibit errors within a 5% margin, a few runs, notably Run 7, Run 11, Run 20, and Run 37, show larger deviations, suggesting that the model's prediction may be less precise under certain conditions. The highest experimental Sqrt(MRR) value observed was 0.5449 g/min during Run 26, typically achieved at higher current levels and longer pulse-on times. It is noted that a higher percentage of Al_2O_3 in the powder mixture (50%-60%) slightly enhances the material removal rate. A higher percentage of Al_2O_3 in the powder mixture slightly enhances the material removal rate (MRR) because Al_2O_3 particles possess higher hardness, toughness, and thermal conductivity than SiO_2 particles [42]. During the NPMEDM process, the suspended Al_2O_3 particles help stabilize and intensify the electrical discharges between the tool and the workpiece by acting as conductive bridges [43,44]. This results in stronger and more consistent sparks, leading to more effective erosion of the workpiece material [45]. Additionally, the superior thermal conductivity of Al_2O_3 promotes efficient heat distribution across the machining zone, supporting continuous melting and material removal. In contrast, a higher content of SiO_2, being softer and less conductive, tends to absorb some of the spark energy, reducing machining efficiency. Therefore, increasing the Al_2O_3 proportion in the powder mixture improves the overall machining performance by facilitating faster and deeper material removal [46]. Figures 3(a) and 3(b) give a predictable and real MMR.

Table 8 presents the prediction accuracy of the Electrode Wear Rate (EWR) for the NPMEDM process, based on 50 experimental runs involving different machining parameters such as peak current (Ip), pulse-on time (Ton), pulse-off time (Toff), powder concentration, and the Al_2O_3:SiO_2 powder mix ratio. The experimental and predicted EWR values are compared, and the error ratio (Exp./Pred.) is calculated to assess the prediction performance. Overall, the prediction model shows a reasonable degree of accuracy, although the variation in error is slightly larger compared to the previous MRR prediction table. The error values in most cases range between 0.7 and 1.3, with a few exceptions like Run 16, where the error reaches 1.6349, indicating a larger mismatch. In general, the model can predict EWR trends with moderate accuracy. Still, there are notable deviations under certain parameter settings, particularly when the machining conditions involve lower currents and specific powder compositions. It can be inferred that electrode wear prediction is more sensitive to variations in process parameters compared to material removal rate prediction, and slight changes in energy input and particle characteristics can lead to considerable differences in electrode wear behavior.

Electrode wear prediction is more sensitive to variations in process parameters than material removal rate prediction because electrode wear depends on the amount of energy delivered and how that energy is absorbed by the electrode material itself[47]. Unlike material removal from the workpiece, which is mainly driven by consistent spark erosion, electrode wear is influenced by many more delicate factors such as localized heating, melting points, thermal conductivity, and the chemical reactivity of the electrode surface with the powder particles and dielectric fluid. Even small changes in peak current, pulse-on time, or the type and concentration of powder particles can significantly alter the energy density at the electrode surface, leading to uneven wear rates [48,49]. Additionally, certain powders like Al_2O_3 and SiO_2 can either shield the electrode from excessive heat or intensify localized sparking, further complicating the wear behavior. Therefore, because electrode wear involves complex thermal, chemical, and electrical interactions, its prediction tends to be more sensitive and less stable than the relatively more straightforward process of material removal from the workpiece [50]. Figures 3(c) and 3(d) give a predictable and real EWR.

Table 7: Prediction Accuracy of Sqrt (MRR) for NPMEDM process

Run	I_p(A)	P_{on}(µs)	P_{off} (µs)	Con. (g/L)	Mix of Al_2O_3%-Balanced SiO_2	Exp. Sqrt (MRR) (g/min)	Pred. MRR (g/min)	Error Exp./Pred.
1	30	250	75	3	50	0.3743	0.4163	0.8992
2	35	100	50	4	40	0.3999	0.4066	0.9835
3	30	150	75	5	50	0.3626	0.3644	0.9952
4	35	100	100	2	40	0.3216	0.3417	0.9411
5	30	150	75	3	50	0.3501	0.3683	0.9508
6	25	200	100	2	60	0.3391	0.3299	1.0278
7	35	100	100	4	60	0.3589	0.3612	0.9935
8	35	200	50	2	40	0.5077	0.4585	1.1075
9	30	150	75	3	50	0.3471	0.3683	0.9426
10	40	150	75	3	50	0.4007	0.4514	0.8877
11	30	50	75	3	50	0.3814	0.3202	1.1911
12	35	200	100	4	40	0.3818	0.3858	0.9897
13	30	150	75	3	30	0.3320	0.3448	0.9627
14	30	150	75	3	50	0.3593	0.3683	0.9757
15	25	100	50	4	60	0.3195	0.3468	0.9213
16	30	150	25	3	50	0.3865	0.4370	0.8844
17	30	150	125	3	50	0.3268	0.2995	1.0913
18	35	200	100	2	40	0.3828	0.3897	0.9822
19	35	100	50	4	60	0.5184	0.4300	1.2055
20	30	150	75	3	50	0.3496	0.3683	0.9493
21	30	150	75	3	50	0.3555	0.3683	0.9654
22	35	100	50	2	60	0.4294	0.4339	0.9897
23	25	100	50	4	40	0.3151	0.3234	0.9744
24	35	200	100	2	60	0.4105	0.4131	0.9936
25	30	150	75	1	50	0.3705	0.3721	0.9957
26	35	200	50	2	60	0.5449	0.4819	1.1307
27	25	200	100	4	60	0.3300	0.3261	1.0121
28	25	100	50	2	60	0.3426	0.3507	0.9770
29	35	200	100	4	60	0.4272	0.4092	1.0439
30	35	100	50	2	40	0.4016	0.4105	0.9785
31	30	150	75	3	50	0.3524	0.3683	0.9570
32	25	100	100	4	60	0.2724	0.2780	0.9797
33	25	100	100	4	40	0.2687	0.2546	1.0553
34	25	100	100	2	40	0.2685	0.2585	1.0388
35	25	200	50	4	40	0.3808	0.3714	1.0253
36	35	100	100	2	60	0.3480	0.3651	0.9531
37	20	150	75	3	50	0.3270	0.2851	1.1469
38	35	200	50	4	40	0.5075	0.4546	1.1165
39	35	200	50	4	60	0.4770	0.4780	0.9978
40	25	100	100	2	60	0.2902	0.2819	1.0293
41	30	150	75	3	50	0.3499	0.3683	0.9500
42	30	150	75	3	50	0.3545	0.3683	0.9628
43	35	100	100	4	40	0.3211	0.3378	0.9505
44	25	200	50	2	60	0.4100	0.3987	1.0283
45	25	200	50	4	60	0.3562	0.3948	0.9022
46	25	200	100	2	40	0.3165	0.3065	1.0328
47	30	150	75	3	70	0.3722	0.3917	0.9501
48	25	200	50	2	40	0.3805	0.3753	1.0140
49	25	100	50	2	40	0.3170	0.3273	0.9687
50	25	200	100	4	40	0.3148	0.3026	1.0402
							Mean	1.0008
							Std. Dev.	0.0710
							C.V	0.0710

Table 9 presents the prediction accuracy of the surface roughness (Ra) for the NPMEDM process across 50 experimental runs, varying parameters such as peak current (Ip), pulse-on time (Ton), pulse-off time (Toff), powder concentration, and Al_2O_3:SiO_2 powder mixture ratio. Comparing the experimental and predicted Ra values shows that the prediction model performs with generally high accuracy. Most error ratios (Exp./Pred.) are very close to 1, typically between 0.8 and 1.05, indicating strong agreement between experimental and predicted results. Overall, the results indicate that the surface roughness prediction is reliable, and the model captures the influence of the process parameters well. This also implies that surface roughness, in this NPMEDM setup, behaves more predictably than EWR, with smaller deviations from model predictions. The small variations observed might be attributed to minor effects of powder concentration and discharge energy, which affect surface characteristics like micro-crack density and molten material re-solidification [10].

Table 8: Prediction Accuracy of EWR for NPMEDM process

Run	I_p(A)	P_{on} (µs)	P_{off} (µs)	Con. (g/L)	Mix of Al_2O_3% - balanced SiO_2	Exp. EWR (g/min)	Pred. EWR (g/min)	Error Exp./Pred.
1	30	250	75	3	50	0.0041	0.0048	0.8542
2	35	100	50	4	40	0.0067	0.0055	1.2182
3	30	150	75	5	50	0.0060	0.0052	1.1538
4	35	100	100	2	40	0.0074	0.0057	1.2982
5	30	150	75	3	50	0.0057	0.0048	1.1875
6	25	200	100	2	60	0.0050	0.0042	1.1905
7	35	100	100	4	60	0.0060	0.0071	0.8451
8	35	200	50	2	40	0.0012	0.0011	1.0909
9	30	150	75	3	50	0.0057	0.0048	1.1875
10	40	150	75	3	50	0.0010	0.0014	0.7143
11	30	50	75	3	50	0.0009	0.0011	0.8182
12	35	200	100	4	40	0.0035	0.004	0.8750
13	30	150	75	3	30	0.0052	0.0047	1.1064
14	30	150	75	3	50	0.0059	0.0048	1.2292
15	25	100	50	4	60	0.0047	0.006	0.7833
16	30	150	25	3	50	0.0103	0.0063	1.6349
17	30	150	125	3	50	0.0008	0.0012	0.6667
18	35	200	100	2	40	0.0039	0.0036	1.0833
19	35	100	50	4	60	0.0091	0.0086	1.0581
20	30	150	75	3	50	0.0058	0.0048	1.2083
21	30	150	75	3	50	0.0059	0.0048	1.2292
22	35	100	50	2	60	0.0086	0.0082	1.0488
23	25	100	50	4	40	0.0015	0.0019	0.7895
24	35	200	100	2	60	0.0083	0.0067	1.2388
25	30	150	75	1	50	0.0023	0.0024	0.9583
26	35	200	50	2	60	0.0103	0.0102	1.0098
27	25	200	100	4	60	0.0051	0.0053	0.9623
28	25	100	50	2	60	0.0046	0.0047	0.9787
29	35	200	100	4	60	0.0086	0.0084	1.0238
30	35	100	50	2	40	0.0075	0.0073	1.0274
31	30	150	75	3	50	0.0059	0.0058	1.0172
32	25	100	100	4	60	0.0035	0.0036	0.9722
33	25	100	100	4	40	0.0015	0.0015	1.0000
34	25	100	100	2	40	0.0016	0.0015	1.0667
35	25	200	50	4	40	0.0007	0.0008	0.8750
36	35	100	100	2	60	0.0059	0.0058	1.0172
37	20	150	75	3	50	0.0042	0.0043	0.9767
38	35	200	50	4	40	0.0011	0.0012	0.9167
39	35	200	50	4	60	0.0106	0.0105	1.0095
40	25	100	100	2	60	0.0034	0.0032	1.0625
41	30	150	75	3	50	0.0058	0.0057	1.0175
42	30	150	75	3	50	0.0059	0.0058	1.0172
43	35	100	100	4	40	0.0066	0.0065	1.0154
44	25	200	50	2	60	0.0063	0.0065	0.9692
45	25	200	50	4	60	0.0065	0.0062	1.0484
46	25	200	100	2	40	0.0007	0.0008	0.8750
47	30	150	75	3	70	0.0065	0.0067	0.9701
48	25	200	50	2	40	0.0007	0.0006	1.1667
49	25	100	50	2	40	0.0017	0.0016	1.0625
50	25	200	100	4	40	0.0006	0.0005	1.2000
							Mean	1.0345
							Std. Dev.	0.1664
							C.V	0.1608

The results imply that surface roughness (Ra) behaves more predictably compared to electrode wear rate (EWR) in the NPMEDM setup because the deviations between the experimental and predicted values for Ra are consistently small, with most errors close to1 [51]. This suggests that surface roughness is primarily governed by the controlled input parameters (such as discharge current, pulse durations, and powder concentration) in a systematic and repeatable way [52]. In contrast, EWR is influenced by more complex, less predictable factors such as localized electrode erosion, thermal stresses, and chemical reactions during sparking, which can introduce random variability that the model cannot easily capture [53]. As a result, Ra shows a more stable and direct relationship with the process settings, leading to smaller deviations from model predictions. At the same time, EWR remains more erratic and harder to predict accurately [54].

Table 9: Prediction Accuracy of Ra for the NPMEDM process

Run	I_p (A)	P_{on} (µs)	P_{off} (µs)	Con. (g/L)	Mix of Al_2O_3% - balanced SiO_2	Exp. Ra (µm)	Pred. Ra (µm)	Error Exp./Pred.
1	30	250	75	3	50	4.527	5.474	0.827
2	35	100	50	4	40	4.949	5.002	0.989
3	30	150	75	5	50	5.589	5.704	0.980
4	35	100	100	2	40	6.801	6.839	0.994
5	30	150	75	3	50	5.712	5.455	1.047
6	25	200	100	2	60	5.185	5.009	1.035
7	35	100	100	4	60	6.752	6.902	0.978
8	35	200	50	2	40	4.407	4.619	0.954
9	30	150	75	3	50	5.498	5.455	1.008
10	40	150	75	3	50	6.289	5.781	1.088
11	30	50	75	3	50	5.361	5.437	0.986
12	35	200	100	4	40	6.499	6.310	1.030
13	30	150	75	3	30	5.777	5.586	1.034
14	30	150	75	3	50	5.488	5.455	1.006
15	25	100	50	4	60	5.048	5.178	0.975
16	30	150	25	3	50	4.827	4.762	1.014
17	30	150	125	3	50	4.954	6.148	0.806
18	35	200	100	2	40	6.318	6.097	1.036
19	35	100	50	4	60	4.820	4.875	0.989
20	30	150	75	3	50	5.564	5.455	1.020
21	30	150	75	3	50	5.637	5.455	1.033
22	35	100	50	2	60	4.622	4.639	0.996
23	25	100	50	4	40	5.163	5.269	0.980
24	35	200	100	2	60	6.177	5.926	1.042
25	30	150	75	1	50	4.874	5.207	0.936
26	35	200	50	2	60	4.311	4.484	0.961
27	25	200	100	4	60	5.465	5.307	1.030
28	25	100	50	2	60	4.830	4.894	0.987
29	35	200	100	4	60	6.389	6.176	1.035
30	35	100	50	2	40	4.737	4.803	0.986
31	30	150	75	3	50	5.602	5.455	1.027
32	25	100	100	4	60	5.418	5.085	1.065
33	25	100	100	4	40	5.523	5.213	1.059
34	25	100	100	2	40	5.222	4.938	1.058
35	25	200	50	4	40	6.293	6.019	1.046
36	35	100	100	2	60	6.433	6.639	0.969
37	20	150	75	3	50	3.954	4.130	0.9574
38	35	200	50	4	40	4.607	4.804	0.959
39	35	200	50	4	60	4.500	4.706	0.956
40	25	100	100	2	60	5.127	4.774	1.074
41	30	150	75	3	50	5.552	5.455	1.018
42	30	150	75	3	50	5.519	5.455	1.012
43	35	100	100	4	40	6.866	7.066	0.972
44	25	200	50	2	60	5.975	5.687	1.051
45	25	200	50	4	60	6.184	5.957	1.038
46	25	200	100	2	40	5.333	5.144	1.037
47	30	150	75	3	70	5.501	5.324	1.033
48	25	200	50	2	40	6.082	5.785	1.051
49	25	100	50	2	40	4.941	5.022	0.984
50	25	200	100	4	40	5.565	5.405	1.030
							Mean	1.0036
							Std. Dev.	0.0525
							C.V	0.0523

4.3 ANOVA Test for MRR, EWR, and Ra

Table 10 and Figure 4 present the ANOVA test results for the MRR output parameter. This table and figure include the Mean Square, Sum of Squares, degrees of freedom (df), F-value, and P-value. The mean square value can be calculated by dividing the sum of the squared values of each output characteristic by the degrees of freedom (df). The F-value was calculated by dividing the Mean Square of the terms by the Mean Square of the residuals.

Table 10: ANOVA test for MRR Response

Source	Sum of Squares	df	Mean Square	F-value	p-value
Model	0.1452	5	0.0290	33.79	< 0.0001
A-Current	0.0692	1	0.0692	80.52	< 0.0001
B-Pulse on	0.0231	1	0.0231	26.82	< 0.0001
C-Pules off	0.0473	1	0.0473	55.05	< 0.0001
D-Concentration	0.0002	1	0.0002	0.1746	0.6781
E-Mix of Al%-Si	0.0055	1	0.0055	6.39	0.0152
Residual	0.0378	44	0.0009		
Lack of Fit	0.0377	37	0.0010	65.26	< 0.0001
Pure Error	0.0001	7	0.0000		
Cor Total	0.1830	49			

The model is considered significant due to its F-value of 33.79. The substantial F-value possesses a 0.01% likelihood of being attributable to random variation. Model terms are deemed significant when P-values are below 0.0500. A (Current), B (Pulse duration), C (Pulse cessation duration), and E (Mixing ratio) are significant parameters of the model. The model terms are insignificant if the value exceeds 0.1000. Model reduction may enhance your model if it has numerous insignificant terms, except those necessary for preserving hierarchy. The F-value of 65.26 signifies a considerable lack of fit. A substantial Lack of Fit F-value has a 0.01% likelihood of being attributable to random variation. A substantial lack of fit is unfavorable as the model must conform adequately.

Figure 4 illustrates that the primary influencing component affecting MRR is current, with a contribution percentage of 37.810%. The percentages for the other parameters were 12.595% for pulse on and 20.850% for pulse off, respectively. The current is the predominant factor influencing the enhancement of the metal removal rate, as previously stated. An increase in current results in a greater concentration of energy in the operational zone, thereby augmenting the likelihood of metal melting and subsequent removal. This process necessitates a substantial pulse on time, coupled with an adequate pulse off time, to facilitate the expulsion of molten metal from the operational area prior to re-solidification.

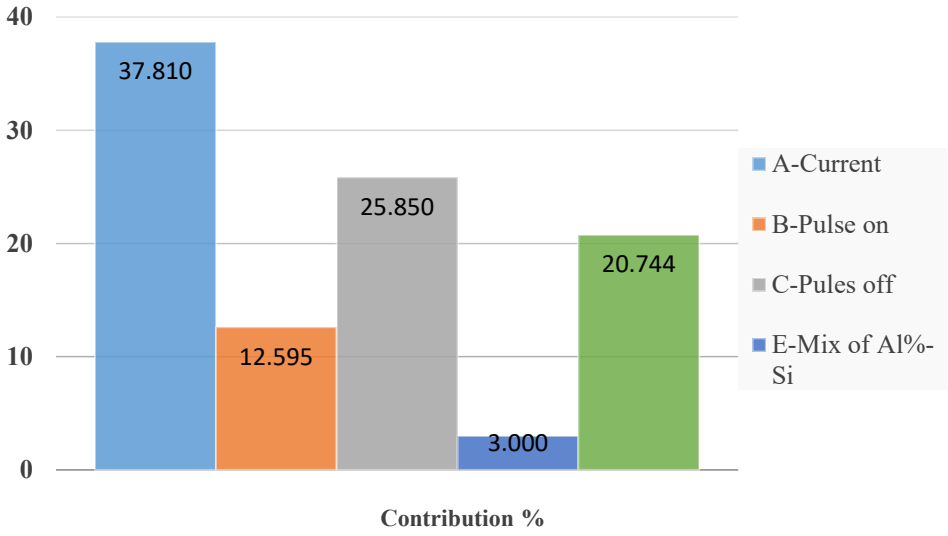

Figure 4: The contribution of parameters to MRR

Table 11 and Figure 5 present the ANOVA test results for the Ra output parameter. These tables and figures include the Mean Square, Sum of Squares, degrees of freedom (df), F-value, and P-value. The mean square value can be calculated by dividing the sum of the squared values of each output characteristic by the degrees of freedom (df). The F-value was calculated by dividing the Mean Square of the terms by the Mean Square of the residuals.

Table 11: ANOVA test for Ra Response

Source	Sum of Squares	df	Mean Square	F-value	p-value
Model	18.07	15	1.20	7.25	< 0.0001
A-Current	1.06	1	1.06	6.37	0.0165
B-Pulse on	0.0034	1	0.0034	0.0206	0.8867
C-Pules off	4.80	1	4.80	28.91	< 0.0001
D-Concentration	0.6175	1	0.6175	3.72	0.0622
E-Mix of Al%-Si	0.1719	1	0.1719	1.03	0.3162
AB	1.80	1	1.80	10.82	0.0023
AC	8.99	1	8.99	54.12	< 0.0001
AD	0.0047	1	0.0047	0.0283	0.8673
AE	0.0026	1	0.0026	0.0158	0.9006
BC	0.6216	1	0.6216	3.74	0.0614
BD	0.0004	1	0.0004	0.0024	0.9615
BE	0.0017	1	0.0017	0.0103	0.9197
CD	0.0015	1	0.0015	0.0093	0.9239
CE	0.0027	1	0.0027	0.0160	0.9000
DE	0.0027	1	0.0027	0.0160	0.9000
Residual	5.65	34	0.1661		
Lack of Fit	5.61	27	0.2076	35.87	< 0.0001
Pure Error	0.0405	7	0.0058		
Cor Total	23.72	49			

The model is considered significant due to its F-value of 7.25. The substantial F-value has a 0.01% likelihood of being attributable to random variation. Model terms are deemed significant when P-values are below 0.0500. A (Current), C (Pulse off

time), AB (Current interaction with Pulse on time), and AC (Current interaction with Pulse off time) are significant terms in the model. The model terms are insignificant if the value exceeds 0.1000. Model reduction may enhance your model if it has numerous insignificant terms, except those necessary for preserving hierarchy. The F-value of 35.87 signifies a considerable lack of fit. A substantial Lack of Fit F-value has a 0.01% likelihood of being attributed to random variation. A substantial lack of fit is unfavorable as the model must conform appropriately.

Figure 5 indicates that pulse off is the most significant parameter influencing Ra, contributing 20.239%. The contributions of the other parameters are 7.573% for current interaction with pulse on and 37.893% for current interaction with pulse off. The primary factor influencing surface roughness is the pulse duration; an increase in this duration results in a decrease in surface roughness, as previously stated, because it facilitates the expulsion of molten metal from the operational region, enhancing surface leveling and diminishing the pulse duration results in the elimination of pits that may form on the treated surface, hence lowering surface roughness, particularly when employing a lower current intensity.

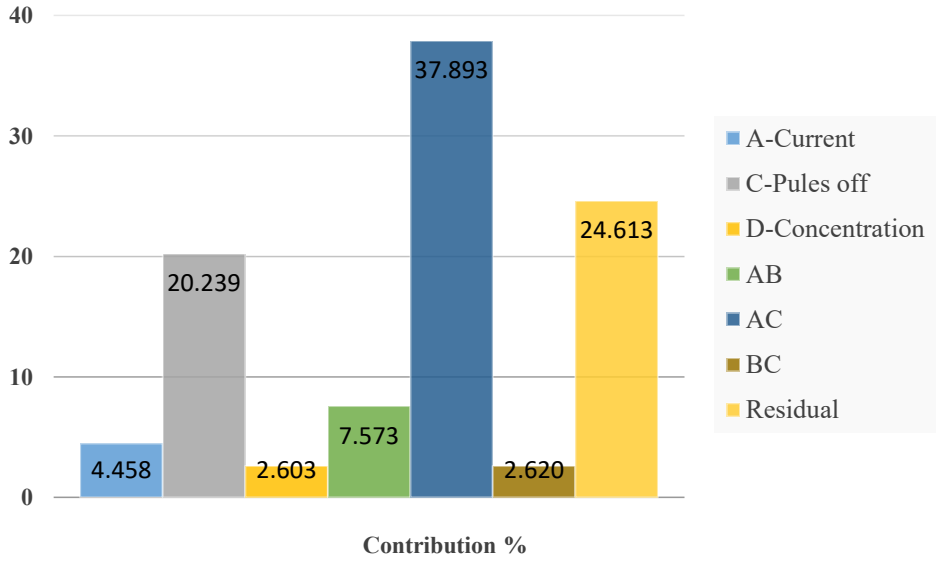

Figure 5: The percentage contribution of parameters to Ra

Table 12 and Figure 6 present the ANOVA test results for the EWR output parameter. These tables and figures include the Mean Square, Sum of Squares, degrees of freedom (df), F-value, and P-value. The mean square value can be calculated by dividing the sum of the squared values of each output characteristic by the degrees of freedom (df). The F-value was calculated by dividing the Mean Square of the terms by the Mean Square of the residuals.

Table 12: ANOVA for EWR Response

Source	Sum of Squares	df	Mean Square	F-value	p-value
Model	0.0002	5	0.0000	7.80	< 0.0001
A-Current	0.0001	1	0.0001	13.70	0.0006
B-Pulse on	1.600E-08	1	1.600E-08	0.0034	0.9538
C-Pules off	0.0000	1	0.0000	4.53	0.0390
D-Concentration	1.089E-06	1	1.089E-06	0.2313	0.6329
E-Mix of Al%-Si	0.0001	1	0.0001	20.55	< 0.0001
Residual	0.0002	44	4.708E-06		
Lack of Fit	0.0002	37	5.597E-06	712.33	< 0.0001
Pure Error	5.500E-08	7	7.857E-09		
Cor Total	0.0004	49			

The model is considered significant due to its F-value of 7.80. The substantial F-value has a 0.01% likelihood of being attributable to random variation. Model terms are deemed significant when P-values fall below 0.0500. A (Current), C (Pulse off time), and E (Mixing ratio) are significant parameters in this context. The model terms are irrelevant if the value exceeds 0.1000. Model reduction may enhance your model if it has numerous insignificant terms, except those necessary for preserving hierarchy. The significant lack of fit is evidenced by an F-value of 712.33. A substantial Lack of Fit F-value has a 0.01% likelihood of being attributable to random variation. A substantial lack of fit is unfavorable, as the model is required to conform.

Figure 6 illustrates that the primary factors affecting EWR were the current and powder mixing ratios, each contributing 25.589% to the overall outcome. The current is the predominant component influencing the tool's wear rate due to its concentration in the operational zone. Nonetheless, we observe the influence of additional factors with equivalent effects, namely concentration and mixing rate. An increase in concentration results in more particles being transported to the operational area, thereby transferring a larger charge, adversely impacting the tool's wear rate. Similarly, the quality of these particles also exerts a comparable negative influence, as previously indicated in the results.

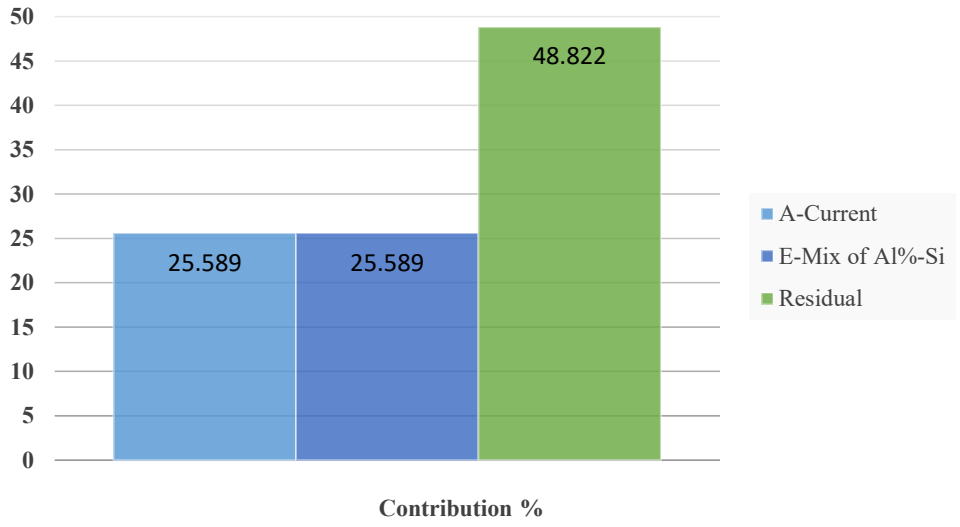

Figure 6: The percentage contribution of parameters to EWR

4.4 Parametric analysis of MRR, EWR, and Ra

The peak current (Ip), pulse duration (Pon), pulse interval (Poff), nanopowder concentration, and nanopowder mixing ratio. Various factors have been examined to determine their influence on the Material Removal Rate (MRR) in the application of NPMEDM for modifying stainless steel 304L surfaces. Utilize statistical software to generate 3D contour diagrams. Three-dimensional response contour diagrams offer adequate information concerning the relationship between input process parameters and material removal rate (MRR). This study employs response surface methodology (RSM) to examine the influence of nanopowder concentration and mixing ratio on the maximum material removal rate (MRR), while maintaining the values of three other parameters constant. Figure 7(a) illustrates that the constants are Ip (35 Amperes), Pon (200 microseconds), and the default value Poff (50 microseconds) in the 3D contour graphic.

The MRR consistently rises to its peak value when the concentration of Al_2O_3 reaches 2 g/L and the mixing ratio is elevated to 60%. An explanation for the observed boost in Material Removal Rate (MRR) following the alteration in mixing ratio, which subsequently elevates the quantity of Al_2O_3 nanoparticles, is that a greater amount of energy may be accessible for discharge within the sparking region. This increased energy availability promotes the melting and evaporation of work materials. The 40% mixing ratio of Al_2O_3 adversely affects the Material Removal Rate (MRR) due to the minimal discharge energy delivered to the surface area at a low concentration (2 g/L), while maintaining the default parameters of Ip (25 Amp.), Pon (100 µs), and Poff (100 µs). Figure 7(b) is a three-dimensional contour diagram illustrating this. The concentration of nanopowder, mixing ratio, peak current (Ip), pulse on time (Pon), and pulse off time (Poff). They have all been examined to ascertain their potential influence on the Surface Roughness (Ra) when the surface of stainless steel 304L is changed using NPMEDM. 3D contour diagrams are generated using the statistical program. Three-dimensional response contour diagrams offer adequate information concerning the relationship between input process parameters and Ra. This work employs response surface methodology (RSM) to examine the influence of Nanopowder concentration and mixing ratio on the maximum surface roughness (Ra), while maintaining the values of the other three parameters: Ip (35 Amp.), Pon (100 µs), and Poff (100 µs), as illustrated in Figure 7(c).

The Ra consistently escalates to its peak value when the concentration of Al_2O_3 reaches four g/L and the mixing ratio is elevated to 40%. The elevated Ra following the alteration in the mixing ratio, which raises the quantity of Al2O3 nanoparticles, is due to additional energy being accessible for discharge within the sparking region. This increased energy availability promotes the melting and evaporation of work materials. Figure 7(d) 3D contour diagram distinctly demonstrates the impact of a 50% Al_2O_3 mixing ratio on Ra at its minimum value, since the discharge energy imparted to the surface area is negligible and corresponds with a reduction in concentration to (3 g/L). The values of Ip (20 Amperes), Pon (150 microseconds), and Poff (75 microseconds) remain at their normal settings.

Response surface methodology (RSM) is employed in Figure 7(e) to generate a 3D contour diagram illustrating the impact of nanopowder concentration and nanopowder mixing ratio on EWR, while keeping the default levels of Ip, Pon, and Poff at 35 Amp, 200 µs, and 50 µs, respectively. The correlation between Nanopowder concentration and mixing ratio indicates that the maximum EWR varies with the mixing ratio up to 60%, corroborating the hypothesis that, at a fixed concentration (4 g/L), a sustained increase in EWR is expected. The elevated expulsion energy associated with a larger mixing ratio of Al_2O_3, which facilitates the melting and vaporization of materials and tool components in the machining area, is often correlated with the observed increase in (EWR) at increased concentrations. The concentration and mixing ratio of nanopowder dictate the energy released during the electromagnetic dipole moment NPMEDM. Consequently, the region is demonstrating a significant maximum. Nanoparticles possess the highest discharge energy value. Figure 7(f) presents a three-dimensional contour plot demonstrating the reduced electrode wear rate observed with a decreased mixing ratio of Al_2O_3 (40%), while sustaining the Ip (25 Amp), Pon (200 µs), and Poff (100 µs). This low EWR value, while maintaining a concentration of 4 g/L, can be elucidated by noting that a reduction in the discharge energy conveyed by nanoparticles corresponds with a drop in the quantity of electrode material that is melted and evaporated.

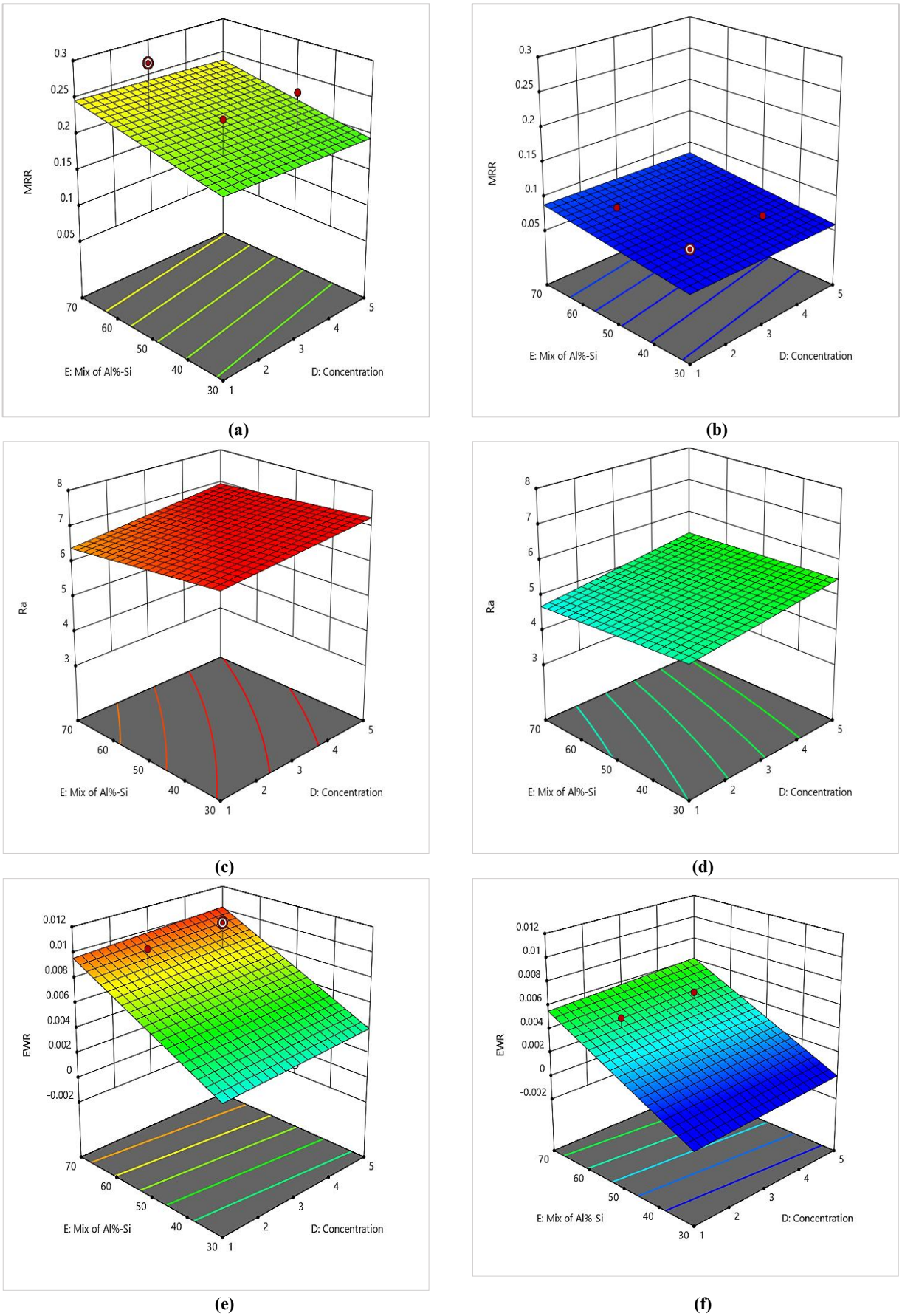

Figure 7: a) Maximum MRR vs. Concentrated and mixed Nanopowder contour diagram b) Minimum MRR vs. Concentrated and mixed Nanopowder contour diagram c) Maximum Ra vs. Concentrated and mixed Nanopowder contour diagram d)Minimum Ra vs. Concentrated and mixed Nanopowder contour diagram e) Maximum EWR vs. Concentrated and mixed Nanopowder contour diagram f)Minimum EWR vs. Concentrated and mixed Nanopowder contour diagram

5. Conclusion

This study analyzes the output responses of Electrical Discharge Machining (EDM), including Surface Roughness (SR), Material Removal Rate (MRR), and Electrode Wear Rate (EWR), for conventional EDM and Nano-Particle-Mixed EDM (NPMEDM). Al2O3 and SiO2 nanoparticles exhibit electrical conductivity and physical properties that diminish the breakdown strength of kerosene and reduce spark delay time, while the material removal rate increases with the concentration of nanoparticles in the kerosene dielectric fluid. This results in the thermal conductivity of nanofluid being significantly greater than traditional dielectrics, enhancing the material removal rate. It has been observed that the Material Removal Rate (MRR) increases with higher discharge currents. Enhancing the proportion of Al2O3 particles during a discharge current of 35 A, with a particle concentration of 2 g/l, a pulse on time of 200 µs, and a pulse off time of 50 µs, results in a 13% improvement in the material removal rate at Run No. 26. Ra diminishes with increased discharge currents; by lowering the discharge current to 20 A, the particle concentration to 3 g/l, the pulse on time to 150 µs, and the pulse off time to 75 µs, the relative composition of aluminum oxide particles is reduced to 50%, yielding an approximate 4.5% enhancement in Ra at Run No. 37. The EWR diminishes with elevated discharge currents; by augmenting the discharge current to 25 A, the particle concentration to 4 g/l, the pulse on time to 200 µs, and the pulse off time to 100 µs, the relative composition of aluminum oxide particles is reduced to 40%, yielding an approximate 33.3% enhancement in EWR at Run No. 50, as determined experimentally using the Design Expert 11 software. The critical variables for MRR are current at 37.8%, pulse on at 12.6%, nanopowder concentration at 3%, and pulse off at 25.85%. The mixing ratio parameter exerts no significant influence on MRR. The critical elements for EWR are the current at 25.5% and the Nanopowder mixing ratio at 25.6%. The critical determinants for Ra include nanopowder concentration, peak current at 4.5%, pulse-off duration at 20.24%, current-pulse duration at 7.6%, and current-pulse off duration at 37.9%.

These findings suggest that NPMEDM can boost productivity, surface quality, and tool life, making it viable for industrial use. Future research should investigate using TiO_2 or CuO nanoparticles and advanced optimisation methods like RSM or Genetic Algorithms to balance machining efficiency and quality. Studies should also include microstructural and hardness investigations of surface integrity in workpiece materials other than stainless steel 304L. Nanoparticle-enhanced dielectric fluid stability, environmental safety, and scalability require long-term investigations. Finally, real-time monitoring and sophisticated control systems could improve EDM uniformity and adaptability, enabling intelligent, next-generation production.

Author contributions

Conceptualization, **Q. Sachit, M. Tawfiq, M. Shamky,** and **W. Abbas**; data curation, **Q. Sachit**; formal analysis, **M. Tawfiq**; investigation, **Q. Sachit**, and **M. Tawfiq**; methodology, **M. Tawfiq,** and **M. Shamky**; project administration, **Q. Sachit**, and **M. Tawfiq**, resources, **M. Shamky,** and **W. Abbas**; software, **W. Abbas**; supervision, **M. Tawfiq**; validation, **M. Tawfiq**, and **W. Abbas**; visualization, **Q. Sachit**; writing—original draft preparation, **Q. Sachit**, and **M. Tawfiq**; writing—review and editing, **W. Abbas**. All authors have read and agreed to the published version of the manuscript.

Funding

This research received no specific grant from any funding agency in the public, commercial, or not-for-profit sectors.

Data availability statement

The data that support the findings of this study are available on request from the corresponding author.

Conflicts of interest

The authors declare that there is no conflict of interest.

References

[1] S. Diyaley, S. Chakraborty, An analysis on the parametric optimization of the electrochemical honing process, J. Adv. Manuf. Syst., 19 (2020) 249-276. https://doi.org/10.1142/S0219686720500134

[2] H. Singh, PK. Jain, DK. Dwivedi, Performance of different abrasive tools in electrochemical honing of coated surfaces, Int. J. Mechatron. Manuf. Syst., 12 (2019) 38-48. https://doi.org/10.1504/IJMMS.2019.097844

[3] M. Y. Khan, P. S. Rao, B. S. Pabla, Investigations on the feasibility of Jatropha curcas oil-based biodiesel for sustainable dielectric fluid in EDM process, Mater. Today Proc., 26 (2020) 335-340. https://doi.org/10.1016/j.matpr.2019.11.325

[4] M. Y. Khan, P. S. Rao, Electrical discharge machining: vital to manufacturing industries, Int. J. Innov. Technol. Explor. Eng., 8 (2019) 1696-1701. http://dx.doi.org/10.35940/ijitee.K1516.0981119

[5] M. Rizwee, P. S. Rao, M. Y. Khan, Recent advancements in electric discharge machining of metal matrix composite materials, Mater. Today Proc., 37 (2021) 2829-2836. https://doi.org/10.1016/j.matpr.2020.08.657

[6] B. K. Baroi, T. Debnath, Jagadish, P. K. Patowari, A State-of-the-Art Review on Surface Modification Techniques in Electric Discharge Machining, North-East Research Conclave, 20 (2022) 165-179. https://doi.org/10.1007/978-981-19-8452-5_14

[7] M. N. Khan, P. S. Rao, Hybridization of electrical discharge machining process, Int. J. Eng. Adv. Technol., 9 (2019) 1059-1065. http://dx.doi.org/10.35940/ijeat.A9477.109119

[8] M. Y. Khan, P. S. Rao, Optimization of process parameters of electrical discharge machining process for performance improvement, Int. J. Innov. Technol. Explor. Eng., 8 (2019) 3830-3836. http://dx.doi.org/10.35940/ijitee.K2262.0981119

[9] S. K. Singh, S. C. Jayswal, Modeling and optimization of EDM Process Parameters on Machining of Inconel 686 using RSM, Int. J. Appl. Eng. Res., 13 (2018) 9335-9344.

[10] V. Prakash, P. Kumar, P. K. Singh, M. Hussain, A. K. Das, S. Chattopadhyaya, Micro-electrical discharge machining of difficult-to-machine materials: a review, Proc. Inst. Mech. Eng., Part B: J. Eng. Manuf., 233 (2019) 339-370. https://doi.org/10.1177/0954405417718591

[11] T. Y. Saindane, H. G. Patil, Electrical Discharge Machining–A State of Art, Int. j. innov. sci. eng. technol., 3 (2016) 262-266.

[12] S. D. Gattu, J. Yan, Micro Electrical discharge machining of ultrafine particle type tungsten carbide using dielectrics mixed with various powders, Micromachines, 13 (2022) 998. https://doi.org/10.3390/mi13070998

[13] A. Taherkhani, M. A. Ilani, F. Ebrahimi, P. N. Huu, B. T. Long, P. Van Dong, N. C. Tam, N. D. Minh, N. Van Duc, Investigation of surface quality in Cost of Goods Manufactured (COGM) method of μ-Al_2O_3 Powder-Mixed-EDM process on machining of Ti-6Al-4V. Int. J. Adv. Manuf. Technol., 116 (2021) 1783-1799. https://doi.org/10.1007/s00170-021-07573-7

[14] D. Kumar, V. K. Pathak, R. Singh, Effect of powder mixed dielectric medium in electrical discharge machining–A review, Mater. Today Proc., 62 (2022) 1596-1600. https://doi.org/10.1016/j.matpr.2022.03.391

[15] T. L. Banh, H. P. Nguyen, C. Ngo, D. T. Nguyen, Characteristics optimization of powder mixed electric discharge machining using titanium powder for die steel materials, Proc. Inst. Mech. Eng., Part E: J. Process Mech. Eng., 232 (2018) 281-298. https://doi.org/10.1177/0954408917693661

[16] M. U. Farooq, H. A. Bhatti, M. Asad, M. S. Kumar, S. Zahoor, A. M. Khan, Surface generation on titanium alloy through powder-mixed electric discharge machining with a focus on bioimplant applications, Int. J. Adv. Manuf. Technol., 122 (2022) 1395-1411.https://doi.org/10.1007/s00170-022-09927-1

[17] S. Mohanty, A. Mishra, B. K. Nanda, B. C. Routara, Multi-objective parametric optimization of nano powder mixed electrical discharge machining of AlSiCp using response surface methodology and particle swarm optimization, Alexandria Eng. J., 57 (2018) 609-619. https://doi.org/10.1016/j.aej.2017.02.006

[18] A. Y. Joshi, A. Y. Joshi, A systematic review on powder mixed electrical discharge machining, Heliyon, 5 (2019) e02963, https://doi.org/10.1016/j.heliyon.2019.e02963

[19] V. D. Bui, J. W. Mwangi, A. Schubert, Powder mixed electrical discharge machining for antibacterial coating on titanium implant surfaces, J. Manuf. Processes., 44 (2019) 261-270. https://doi.org/10.1016/j.jmapro.2019.05.032

[20] S. Ramesh, M. P. Jenarthanan, Investigation of powder mixed EDM of nickel-based superalloy using cobalt, zinc and molybdenum powders, Trans. Indian Inst. Met., 74 (2021) 923-936. https://doi.org/10.1007/s12666-020-02170-w

[21] J. Shiek, J. Sairam, P. A. Mouda, Parameter optimization in the enhancement of MRR of titanium alloy using newer mixing method in PMEDM process, J. Eng. Appl. Sci., 70 (2023). https://doi.org/10.1186/s44147-023-00230-8

[22] B. K. Matanda, V. Patel, U. Joshi, A. Joshi, A review on powders used for PMEDM machining process, AIP Conf. Proc., 3107 (2024). https://doi.org/10.1063/5.0212305

[23] P. R. Dewan, P. K. Kundu, R. Phipon, Powder mixed electric discharge machining–A review, AIP Conf. Proc., 2273 (2020). https://doi.org/10.1063/5.0025268

[24] B. T. Long, N. Cuong, N. H. Phan, P. Janmanee, Machining properties evaluation of copper and graphite electrodes in PMEDM of SKD61 steel in rough machining, Int. J. Eng. Adv. Technol., 4 (2015) 193-202. https://doi.org/10.1504/IJMMS.2012.049971

[25] N. Mookam, P. Sunasuan, T. Madsa, P. Muangnoy, S. Chuvaree, Effects of graphite and boron carbide powders mixed into dielectric fluid on electrical discharge machining of SKD 11 tool steel, Arabian J. Sci. Eng., 46 (2021) 2553-2563. https://doi.org/10.1007/s13369-020-05156-4

[26] R. K. Patel, M. K. Pradhan, Machining of nickel-based super alloy Inconel 718 using alumina nanofluid in powder mixed electric discharge machining, Mater. Res. Express, 10 (2023) 036501. https://doi.org/10.1088/2053-1591/acbae8

[27] K. A. Pillai, P. Hariharan, Experimental investigation on surface and machining characteristics of micro ED milling of Ti-6Al-4 V with different nano powder mixed dielectrics, Silicon, 14 (2022) 2871-2894. https://doi.org/10.1007/s12633-021-01041-3

[28] S. K. Chaubey, S. Singh, A. Singh, Some investigations into machining of AISI D2 tool steel using wire electro discharge machining (WEDM) process, Mater. Today Proc., 5 (2018) 24347-24357. https://doi.org/10.1016/j.matpr.2018.10.230

[29] M. P. Jahan, M. Rahman, Y. S. Wong, Study on the nano-powder-mixed sinking and milling micro-EDM of WC-Co, Int. J. Adv. Manuf. Tech., 53 (2011) 167-180. https://doi.org/10.1007/s00170-010-2826-9

[30] P. Sivaprakasam, P. Hariharan, Surface characteristics of nano powder mixed micro-wire electrical discharge machining on inconel alloy, Mater. Today Proc., 38 (2021) 494-498.https://doi.org/10.1016/j.matpr.2020.02.329

[31] S. Patil, R. Kulkarni, M. Patil, V. R. Malik, Investigations on material removal and tool wear rate of silver nanoparticles coated copper electrodes for electric discharge machining, Adv. Mater. Process. Technol., 10 (2023) 3067-3095. https://doi.org/10.1080/2374068X.2023.2194519

[32] S. Mohal, H. Kumar, Parametric optimization of multiwalled carbon nanotube-assisted electric discharge machining of Al-10% SiCp metal matrix composite by response surface methodology, Mater. Manuf. Processes, 32 (2017) 263-273. https://doi.org/10.1080/10426914.2016.1140196

[33] M. Shabgard, B. Khosrozadeh, Investigation of carbon nanotube added dielectric on the surface characteristics and machining performance of Ti–6Al–4V alloy in EDM process, J. Manuf. Processes, 25 (2017) 212-219. https://doi.org/10.1016/j.jmapro.2016.11.016

[34] A. Kumar, A. Mandal, A. R. Dixit, A. K. Das, Performance evaluation of Al2O3 nano powder mixed dielectric for electric discharge machining of Inconel 825, Mater. Manuf. Processes, 33 (2018) 986-995. https://doi.org/10.1080/10426914.2017.1376081

[35] P. Sivaprakasam, P. Hariharan, S. Gowri, Experimental investigations on Nanopowder mixed Micro-Wire EDM process of Inconel-718 alloy. Measurement, 147 (2019) 106844. https://doi.org/10.1016/j.measurement.2019.07.072

[36] Y. Tijjani, High-temperature applications of carbon nanotubes (CNTs)[v]: thermal conductivity of CNTs reinforced silica nanocomposite, Bayero J. Pure App. Sci., 15 (2022) 136-140. https://doi.org/10.4314/bajopas.v15i1.19

[37] Y. Wu, X. Zhang, A. Negi, J. He, G. Hu, S. Tian, J. Liu, Synergistic effects of boron nitride (BN) nanosheets and silver (Ag) nanoparticles on thermal conductivity and electrical properties of epoxy nanocomposites, Polymers., 12 (2020) 426. https://doi.org/10.3390/polym12020426

[38] V. Lalwani, P. Sharma, C. I. Pruncu, D. R. Unune, Response surface methodology and artificial neural network-based models for predicting wire electrical discharge machining performance of Inconel 718 alloys. J. Manuf. Mater. Process., 4 (2020) 44. https://doi.org/10.3390/jmmp4020044

[39] V. Prakash, P. Kumar, P. K. Singh, M. Hussain, A. K. Das, Chattopadhyaya S. Micro-electrical discharge machining of difficult-to-machine materials: a review, Proc. Inst. Mech. Eng. B: J. Eng. Manuf., 233 (2019) 339-370. https://doi.org/10.1177/0954405417718591

[40] S. Jarin, T. Saleh, A. G. Muthalif, M. Y. Ali, M. Bhuiyan, Towards achieving nanofinish on silicon (Si) wafer by µ-wire electro-discharge machining, Int. J. Adv. Manuf. Technol., 99 (2018) 3005-3015. https://doi.org/10.1007/s00170-018-2692-4

[41] D. Thirumalaikumarasamy, V. Balasubramanian, S. S. Sabari, Prediction and optimization of process variables to maximize the Young's modulus of plasma sprayed alumina coatings on AZ31B magnesium alloy, J. Magnesium Alloys, 5 (2017) 133-145.https://doi.org/10.1016/j.jma.2017.02.002

[42] R. Davis, A. Singh, K. Debnath, R. M. Sabino, K. Popat, P. Soares, A. K. Keshri, Borgohain B. Enhanced micro-electric discharge machining-induced surface modification on biomedical Ti-6Al-4V alloy, J. Manuf. Sci. Eng., 144 (2022) 071002. https://doi.org/10.1115/1.4053110

[43] Y. Fang, M. K. Kim, Y. Zhang, Z. Duan, Q. Yuan, J. Suhr, Particulate-reinforced iron-based metal matrix composites fabricated by selective laser melting: A systematic review, J. Manuf. Processes, 74 (2022) 592-639.https://doi.org/10.1016/j.jmapro.2021.12.018

[44] V. S. Kumar, D. Viswanathan, S. Natarajan, Theoretical prediction and FEM analysis of superplastic forming of AA7475 aluminum alloy in a hemispherical die, J. Mater. Process. Technol., 173 (2006) 247-251. https://doi.org/10.1016/j.jmatprotec.2005.04.112

[45] D. He, X. Li, Z. Li, J. Xie, J. Hao, Y. K. Lee, P. Hu, K. Tang, Iso-force rough machining of freeform deep cavities based on volumetric fields, J. Manuf. Processes,. 131 (2024) 1970-1986. https://doi.org/10.1016/j.jmapro.2024.09.104

[46] M. L. Montero-Sistiaga, R. Mertens, B. Vrancken, X. Wang, B. Van Hooreweder, J. P. Kruth, J. Van Humbeeck, Changing the alloy composition of Al7075 for better processability by selective laser melting, J. Mater. Process. Technol., 238 (2016) 437-445. https://doi.org/10.1016/j.jmatprotec.2016.08.003

[47] P. N. Huu, S. Shirguppikar, V. Ganachari, T. Muthuramalingam, L. N. Trong, Optimizing surface quality in PMEDM using SiC powder material by combined solution response surface methodology–Adaptive neuro fuzzy inference system, J. Mech. Behav. Mater., 34 (2025) 20250051. https://doi.org/10.1515/jmbm-2025-0051

[48] P. Ruan, D. Saxena, J. Cao, X. Liu, R. Wang, C. F. Cheung, NASPrecision: Neural Architecture Search-Driven Multi-Stage Learning for surface roughness prediction in ultra-precision machining, Expert Syst. Appl., 262 (2025) 125540. https://doi.org/10.1016/j.eswa.2024.125540

[49] S. Arun, M. Manikandan, J. Joshy, B. Kuriachen, J. Mathew, Numerical modelling and experimental investigations to predict the tool wear of copper electrodes during µ-EDM process, CIRP J. Manuf. Sci. Technol., 55 (2024) 174-187. https://doi.org/10.1016/j.cirpj.2024.09.011

[50] X. Yin, H. Liu, Y. Zhou, Y. Wang, S. Li, Prediction model of material removal rate and surface roughness for silicon single crystal EDM, Tenth International Conference on Mechanical Engineering, Mater. Automation Technol., (MMEAT 2024) 13261 (2024) 698-704. https://doi.org/10.1117/12.3046639

[51] P. Wang, R. X. Gao, R. Yan, A deep learning-based approach to material removal rate prediction in polishing, CIRP annals, 66 (2017) 429-432. https://doi.org/10.1016/j.cirp.2017.04.013

[52] J. Deng, Q. Zhang, J. Lu, Q. Yan, J. Pan, R. Chen, Prediction of the surface roughness and material removal rate in chemical mechanical polishing of single-crystal SiC via a back-propagation neural network, Precis. Eng., 72 (2021) 102-110. https://doi.org/10.1016/j.precisioneng.2021.04.012

[53] Z. Li, D. Wu, T. Yu, Prediction of material removal rate for chemical mechanical planarization using decision tree-based ensemble learning, J. Manuf. Sci. Eng. Mar, 141 (2019) 031003. https://doi.org/10.1115/1.4042051

[54] J. Zhang, Y. Jiang, H. Luo, S. Yin, Prediction of material removal rate in chemical mechanical polishing via residual convolutional neural network, Control Eng. Pract., 107 (2021) 104673. https://doi.org/10.1016/j.conengprac.2020.104673